Ultimate capabilities for few-cycle pulse formation via resonant interaction of XUV radiation with IR-field-dressed atoms

T. R. Akhmedzhanov,[1] M. Yu. Emelin,[2,3] V. A. Antonov,[2,3,*] Y. V. Radeonychev,[2]
M. Yu. Ryabikin,[2,3] and Olga Kocharovskaya[1]

[1]*Department of Physics and Astronomy and Institute for Quantum Studies and Engineering, Texas A&M University,
College Station, Texas 77843-4242, USA*
[2]*Institute of Applied Physics, Russian Academy of Sciences, 46 Ulyanov Street, Nizhny Novgorod 603950, Russia*
[3]*Prokhorov General Physics Institute, Russian Academy of Sciences, 38 Vavilov Street, Moscow 119991, Russia*

We perform an *ab initio* study of the ultimate capabilities and limits of applicability of the method for few-cycle pulse formation via the resonant interaction of extreme ultraviolet (XUV) radiation with atoms dressed by a moderately strong infrared (IR) laser field proposed in two earlier works [Y. V. Radeonychev *et al.*, Phys. Rev. Lett. **105**, 183902 (2010) and V. A. Polovinkin *et al.*, Opt. Lett. **36**, 2296 (2011)]. Taking into account all the multiphoton processes in the systems under consideration on the basis of numerical solution of the three-dimensional time-dependent Schrödinger equation (TDSE) in the single-active-electron approximation, we show the possibilities to produce 1.1-fs pulses from 124.6-nm XUV radiation via the linear Stark effect in atomic hydrogen, as well as 500-as pulses from 58.4-nm XUV radiation via excited-state ionization in helium. We derive a generalized analytical solution, which takes into account the interplay between sub-laser-cycle Stark effect and excited-state ionization and allows us to analyze the results of TDSE calculations. We found that the ultimate intensity of the IR field suitable for few-cycle pulse formation via the linear Stark effect or excited-state ionization is limited by the threshold for atomic ionization from the resonant excited state or the ground state, respectively. We show that the pulses with shorter duration can be produced in the medium of ions with higher values of the ionization potential.

I. INTRODUCTION

Starting from the turn of the millennium [1,2], attosecond physics has become a fascinating branch of modern science, opening the possibility for real-time imaging and steering of electronic motion in atoms, molecules, and solids on its intrinsic time scale [3–9], conceptually similar to the femtosecond optical control of chemical reactions [10].

During recent years, remarkable progress has been achieved in understanding and manipulating the sub-laser-cycle dynamics of the bound and autoionizing atomic states induced by an intense laser field combined with attosecond pulses or pulse trains of the extreme ultraviolet (XUV) radiation produced via high-harmonic generation (HHG) of a replica of the laser field [4,6–8,11–20]. In these studies, the laser field is not strong enough to ionize or excite atoms from their ground state, but it strongly perturbs the excited states resonantly populated by high-harmonic radiation. This perturbation has been visualized directly via the attosecond transient absorption technique [6,17,18]. Due to mutual coherence of the fundamental laser field and its high-order harmonics, the pathways of atomic excitation and ionization through absorption of a higher-harmonic photon or a lower-harmonic photon along with a few photons of the laser field (or, explicitly, the pathways of atomic excitation by different harmonics into the same Floquet state) interfere, leading to beatings of the atomic ionization yield versus the sub-laser-cycle time delay between the harmonic signal and the laser field [11–13,15,17–19] and allowing for the complete transparency of the medium for the resonant XUV radiation [19,20]. However, the possibilities for such investigations and control over the ultrafast intra-atomic dynamics are limited by the nature of the HHG process in gases, which is commonly used for the attosecond pulse formation and dictates the relatively high carrier frequency and low efficiency of generation of the XUV pulses [1,3,8].

Although in recent years both HHG and laser technologies have been considerably advanced, resulting, in particular, in the generation of high-energy (∼1 μJ) isolated attosecond pulses [21], the photon energy of these pulses remains above the ionization potential of both the generating medium and the majority of neutral media, which prevents their being used for nonionizing manipulation of ultrafast intra-atomic and intramolecular processes and impedes investigation of such processes without photoionization. At the same time, the below-threshold harmonics can be produced with generation efficiency up to 1% (which is much higher than that of the above-threshold harmonics used in [21]) under the resonance conditions [22]. However, although the below-threshold harmonics are generated in a comb [23], they are not phase matched with each other and do not constitute attosecond pulses in the time domain. Furthermore, the use of resonantly enhanced HHG and plasma-based x-ray lasers allow for producing XUV and soft x-ray field with high power, exceeding the power of nonresonant high harmonics at the same wavelength. In particular, the transitions from autoionizing states to the ground state of multielectron atoms (ions) allow increasing the intensity of the resonant (above-threshold) harmonic compared to nonresonant ones by two orders of magnitude and achieve 10^{-4} efficiency of a single harmonic generation [24–26], whereas transient inversion on high-frequency transitions of multiply charged ions in

*antonov@appl.sci-nnov.ru

laser-produced plasmas provides an opportunity to generate picosecond pulses of XUV and soft x-ray field with energy up to several mJ [27–30]. However, these sources produce quasimonochromatic radiation, which is not suitable for the time-domain studies of the ultrafast femto- and attosecond processes.

Recently, a method has been proposed which may allow for the conversion of XUV and soft x-ray radiation from these high-energy sources into the attosecond pulses. This method uses the resonant interaction of an incident XUV radiation with an atomic gas dressed by a moderately strong infrared (IR) laser field [31,32] and is based on sub-laser-cycle splitting (due to the linear Stark effect [17,33]) and/or broadening (due to ionization [34,35]) of the excited energy levels, selected and populated by the XUV radiation, under the action of the IR field. The magnitudes of the splitting and broadening of the atomic energy levels oscillate in time and space along with oscillation of the laser-field strength, leading to the multifrequency resonant response of the IR-field-dressed atoms to the (quasimonochromatic) incident XUV radiation. Under the optimal conditions, both Stark splitting of the resonant excited atomic energy level in a hydrogenlike medium [31,36] and rapid quasistatic ionization from the resonant excited state in arbitrary atomic gas [32,37,38] allow for the formation of nearly bandwidth-limited few-femto- or attosecond pulses without external adjustment of phases of the generated sidebands (in contrast with the attosecond pulse formation through HHG, which implies the attochirp compensation [39]). The possibilities to produce both the (quasi-) periodic pulse trains [31,32,36,37] and the isolated attosecond pulses [38] were shown. The efficiency of energy conversion of the XUV field into a pulse train can exceed 75% [36] in the case of pulse formation based on the linear Stark effect and reach 10% in the ionization-switching regime [40]. The discussed approach allows for the formation of attosecond pulses with the carrier frequency below the ionization potential of neutral atoms, molecules, and solids (corresponding to the wavelength range of 50–200 nm), providing an opportunity for the nondestructive subfemtosecond control of the bound electron dynamics [4,6–9]. Proximity of the carrier frequency of the pulses to various resonances in neutral and ionized media holds the promise to use the resonant enhancement of the nonlinear susceptibilities for the implementation of the attosecond pump–attosecond probe experiments [21,41]. Furthermore, the possibility to transform high-energy picosecond pulses of x-ray plasma lasers [27–30,42–44] into the trains or isolated attosecond pulses opens the door for numerous applications in dynamical, high temporal and high spatial resolution element-specific imaging in biochemistry and mateials science [45,46].

The previously obtained results were restricted to three- or two-level models, implying adiabatic approximation for atomic perturbation by the IR field and the resonant approximation for interaction of XUV radiation with atoms. The influence of the IR field on the atomic system was taken into account through space-time variation of instantaneous position and width of the resonant excited atomic energy levels, while interaction of the XUV radiation with atoms, although described dynamically, was considered in few-level models. Although this approach is correct in the limit of a

low frequency and low intensity of the IR field and allows for the analytical solutions, as well as numerical treatment of the propagation problems, it does not allow for determining the ultimate capabilities and the limits of applicability of the method.

In the present paper, we address these questions taking into account all the multiphoton processes in the considered system on the basis of numerical solution of the full three-dimensional time-dependent Schrödinger equation (TDSE) in the single-active-electron approximation. We find the maximal intensity and the minimal wavelength of the laser field suitable for few-femto- and attosecond pulse formation from incident XUV radiation via modulation of the resonant atomic response, as well as the minimal duration of the produced pulses. The mechanisms of pulse formation due to the linear Stark effect [31,36] and the excited-state ionization [32,37,38] are considered for the hydrogen and helium atoms, respectively. The results of numerical calculations are compared to the analytical solutions obtained in [36,37]. In order to analyze the differences between these quasistatic analytical solutions [36,37] and the results of *ab initio* TDSE calculations, we develop a generalized analytical theory, which takes into account a sub-IR-field-cycle space-time variation of the quadratic Stark effect and the excited-state ionization rates. The developed theory allows for distinguishing the differences between the simplified analytical solutions [36,37] and the *ab initio* calculations, which are caused by the interplay between the Stark effect and quasistatic ionization, from those originating from the nonadiabatic processes. Moreover, the generalized theory allows for tracing a transition between the two regimes of pulse formation (based on the linear Stark effect and excited-state ionization) with increasing intensity of the IR field. The performed TDSE calculations are free of most of the assumptions made in theoretical works (restricting the number of levels, neglecting the interaction with a continuum or using the quasistatic approximation for ionization rates, neglecting higher-order Stark effect, etc.) and, thus, provide a direct bridge to an experimental implementation of suggested mechanisms.

The paper is organized as follows. In Sec. II, we analyze the possibilities for ultrashort pulse formation from XUV radiation via Stark splitting of the resonant excited energy level of the atomic hydrogen by a moderately strong IR field of various intensities and wavelengths. In Sec. III, we consider the ionization-switching mechanism of few-cycle attosecond pulse formation from the resonant XUV radiation in helium under the action of a strong IR field. The paper is finalized by a conclusion.

II. FEW-FEMTOSECOND PULSE FORMATION VIA LINEAR STARK EFFECT IN ATOMIC HYDROGEN

Let us consider the propagation of XUV radiation through an optically thin medium of an atomic gas. At the entrance to the medium, $x = 0$, the radiation is monochromatic and its electric field has the form

$$\vec{E}_{\text{inc}}(t) = \tfrac{1}{2}\vec{z}_0 E_0 \exp\{-i\omega_0 t\} + \text{c.c.}, \qquad (1)$$

where E_0 is the incident field amplitude, ω_0 is its angular frequency, and c.c. stands for the complex conjugation. The

radiation (1) is chosen to be near resonant to the transition $|1\rangle \leftrightarrow |2\rangle$ between the ground state and an excited atomic bound state, $\omega_0 \approx \omega_{21}^0$ (where ω_{21}^0 is the frequency of the unperturbed resonant transition).

The medium is simultaneously irradiated by a moderately strong IR laser field,

$$\vec{E}_{\mathrm{IR}}(x,t) = \tfrac{1}{2}\vec{z}_0 E_C \exp\{-i\Omega(t - x/c) + \varphi_0\} + \mathrm{c.c.}, \quad (2)$$

where E_C is the amplitude of the IR field, Ω is its angular frequency, φ_0 is its initial phase ($\varphi_0 = 0$, unless specified otherwise), and c is the speed of light in vacuum. Both the IR field and the XUV radiation propagate along the same direction and are identically polarized. Since in an isotropic gas the polarizations of the fields are not changed, the vector notations will be omitted for now on. Since the medium considered in the paper is optically thin, due to far detuning from the relevant atomic resonances and tiny population of the excited states, the IR field (2) does not suffer from atomic dispersion and traverses the medium without appreciable distortions.

Propagation of the XUV radiation through the medium is described by the wave equation

$$\frac{\partial^2 E_{\mathrm{XUV}}}{\partial x^2} - \frac{1}{c^2}\frac{\partial^2 E_{\mathrm{XUV}}}{\partial t^2} = \frac{4\pi}{c^2}\frac{\partial^2 P_{\mathrm{XUV}}}{\partial t^2}, \quad (3)$$

where E_{XUV} is the XUV radiation strength, $E_{\mathrm{XUV}}(x = 0, t) = E_{\mathrm{inc}}(t)$, and P_{XUV} is the high-frequency polarization of the medium.

Since the characteristic scales of a spatial evolution of XUV radiation in a gas are much larger than its wavelengths, the substitution $t \to \tau \equiv t - x/c$ (within the slowly evolving wave approximation [47,48]) allows for reducing the wave equation (3) to

$$\frac{\partial E_{\mathrm{XUV}}}{\partial x} = -\frac{2\pi}{c}\frac{\partial P_{\mathrm{XUV}}}{\partial \tau}. \quad (4)$$

Finally, in an optically thin medium (when the rescattered field remains much weaker than the incident one) the output radiation transmitted through the medium of thickness L has the form

$$E_{\mathrm{XUV}}(L,\tau) = E_{\mathrm{inc}}(\tau) + E_{\mathrm{Scatt}}(L,\tau),$$
$$E_{\mathrm{Scatt}}(L,\tau) = \frac{2\pi L}{c}\frac{dP_{\mathrm{XUV}}(\tau)}{d\tau}, \quad (5)$$

where $E_{\mathrm{Scatt}}(L,\tau)$ is the resonantly scattered XUV radiation determined by the incident fields (1) and (2).

In a gas, $P_{\mathrm{XUV}}(\tau) = Nd_{\mathrm{XUV}}(\tau)$, where N is the concentration of atoms and $d_{\mathrm{XUV}}(\tau)$ is the high-frequency part of the dipole moment of an individual atom, $d(\tau) = e\langle z(\tau)\rangle$ [where e is the electron charge and $\langle z(\tau)\rangle$ is the expectation value of the active atomic electron displacement along the polarization direction of the field].

In order to get an *ab initio* solution for $d(\tau)$, we numerically solve the three-dimensional TDSE for an atom simultaneously irradiated by the XUV and IR fields (1) and (2):

$$i\hbar\frac{\partial}{\partial t}\psi = (H_0 + V)\psi, \quad (6)$$

where ψ is the wave function of the active electron, $H_0 = -\frac{\hbar^2}{2m}\Delta + U(\vec{r})$ is the unperturbed atomic Hamiltonian (in the case of atomic hydrogen, $U(\vec{r}) = -e^2/r$ corresponds to the

pure Coulomb potential), and $V = e\vec{E}_{\mathrm{IR}}(t) \cdot \vec{r} + e\vec{E}_{\mathrm{XUV}}(t) \cdot \vec{r}$ is the Hamiltonian of atom-field interaction. The solution is obtained using the generalized pseudospectral method [49]. The high-frequency component of the dipole moment $d_{\mathrm{XUV}}(\tau)$ is calculated by filtering out the low-frequency components of the total dipole moment, $d(\tau)$, at the frequencies of low-order harmonics of the IR field and below. An additional filtering is applied for the spectral components with photon energies exceeding the atomic ionization potential, which accounts for a strong photoabsorption of XUV radiation just above the ionization potential.

In the following, the results of TDSE calculations are compared to the analytical solution [36] derived for atomic hydrogen exposed to XUV radiation, which is resonant to the transition $n = 1 \leftrightarrow n = 2$ (where n is the principal quantum number). The analytical solution takes into account the sub-laser-cycle splitting of the excited energy level $n = 2$ due to the linear Stark effect produced by the IR field, but neglects time dependencies of the shift and broadening of the excited energy level due to the quadratic Stark effect and the excited-state ionization, respectively.

In order to analyze the discrepancies between the simplified modeling and TDSE solution, a generalized analytical solution is derived, which takes into account the interplay between the Stark effect and excited-state ionization, as well as the quadratic correction to the alternating-current (ac) linear Stark effect in atomic hydrogen. The analytical solution implies the approximation of slowly varying amplitudes: $F(\tau) = \frac{1}{2}\tilde{F}(\tau)\exp\{-i\omega_0\tau\} + \mathrm{c.c.}$, $|\frac{d\tilde{F}}{d\tau}| \ll \omega_0|\tilde{F}|$, where $F(\tau) = \{E_{\mathrm{XUV}}(L,\tau), E_{\mathrm{Scatt}}(L,\tau), P_{\mathrm{XUV}}(\tau)\}$. Within such an approximation, Eq. (5) takes the form

$$\tilde{E}_{\mathrm{XUV}}(L,\tau) = E_0 + \tilde{E}_{\mathrm{Scatt}}(L,\tau),$$
$$\tilde{E}_{\mathrm{Scatt}}(L,\tau) = i\frac{2\pi\omega_0 L}{c}\tilde{P}_{\mathrm{XUV}}(\tau). \quad (7)$$

The analytical solution for atomic hydrogen is derived within the three-level model, which includes the ground energy level $n = 1$ and the two sublevels of the first excited energy level $n = 2$ selected and populated by the resonant XUV radiation (1). The corresponding atomic states are $|1\rangle = |100\rangle$, $|2\rangle = (|200\rangle + |210\rangle)/\sqrt{2}$, and $|3\rangle = (|200\rangle - |210\rangle)/\sqrt{2}$ (numerals $|nlm\rangle$ label principal, orbital, and magnetic quantum numbers, respectively). In the three-level approximation, the nonresonant interaction of XUV radiation with the medium is neglected, while the slowly varying amplitude of the resonant polarization is given by

$$\tilde{P}_{\mathrm{XUV}}(\tau) = 2Nd_{\mathrm{tr}}[a_{21}(\tau) - a_{31}(\tau)], \quad (8)$$

where N is the concentration of atoms, $d_{\mathrm{tr}} = 2^7 er_B/3^5$ is the dipole moment of the resonant transitions (e is the charge of the electron; r_B is the Bohr radius), and a_{21}, a_{31} are the slowly varying amplitudes of the atomic coherencies ρ_{21}, ρ_{31} at the transitions $|1\rangle \leftrightarrow |2\rangle$ and $|1\rangle \leftrightarrow |3\rangle$, respectively. The coherency amplitudes satisfy the equations

$$\frac{da_{21}}{d\tau} + \{i[\omega_{21}(\tau) - \omega_0] + \gamma_{21}(\tau)\}a_{21} = i\frac{d_{\mathrm{tr}}E_0}{2\hbar},$$
$$\frac{da_{31}}{d\tau} + \{i[\omega_{31}(\tau) - \omega_0] + \gamma_{31}(\tau)\}a_{31} = -i\frac{d_{\mathrm{tr}}E_0}{2\hbar}, \quad (9)$$

where $\omega_{21}(\tau)$, $\omega_{31}(\tau)$ and $\gamma_{21}(\tau)$, $\gamma_{31}(\tau)$ are the instantaneous frequencies and decoherence rates of the transitions $|1\rangle \leftrightarrow |2\rangle$ and $|1\rangle \leftrightarrow |3\rangle$, respectively, which vary in space and time due to the sub-laser-cycle shift and broadening of the energy levels $|2\rangle$ and $|3\rangle$ introduced by the IR field; $\omega_{s1}(\tau) = \omega_{s1}^{(0)} + \Delta E_s(\tau)/\hbar$ and $\gamma_{s1}(\tau) = \gamma_{s1}^{(0)} + w_{\text{ion}}^{(s)}(\tau)/2$, where $\omega_{s1}^{(0)}$ and $\gamma_{s1}^{(0)}$ are the unperturbed frequency and decoherence rate of the transition $|1\rangle \leftrightarrow |s\rangle$, while $\Delta E_s(\tau)$ and $w_{\text{ion}}^{(s)}(\tau)$ are the instantaneous energy shift of the excited state $|s\rangle$ and the ionization rate from it; $\hbar$ is Planck's constant. The perturbation of the ground state $|1\rangle$ by the laser field of intensity relevant to this study is negligible.

In order to find the generalized analytical solution, we use the biharmonic approximation for the dependencies $\omega_{s1}(\tau)$ and $\gamma_{s1}(\tau)$:

$$\omega_{s1}(\tau) = \bar{\omega}_{\text{tr}} \mp \Delta_{\omega}^{(1)} \cos(\Omega\tau) - \Delta_{\omega}^{(2)} \cos(2\Omega\tau), \quad (10a)$$

$$\gamma_{s1}(\tau) = \bar{\gamma}_{\text{tr}} \pm \Delta_{\gamma}^{(1)} \cos(\Omega\tau) + \Delta_{\gamma}^{(2)} \cos(2\Omega\tau), \quad (10b)$$

where the upper and lower signs correspond to $s = 2$ and $s = 3$, respectively. The values $\bar{\omega}_{\text{tr}}$ and $\bar{\gamma}_{\text{tr}}$ characterize the time-averaged position and width of the atomic resonances in the presence of the IR field; $\Delta_{\omega}^{(1)}$ and $\Delta_{\omega}^{(2)}$ are amplitudes of the sweeping of the transition frequencies due to the linear and the quadratic Stark effect, respectively, while $\Delta_{\gamma}^{(1)}$ and $\Delta_{\gamma}^{(2)}$ are variations of ionization rates from the excited states $|2\rangle$ and $|3\rangle$ at the fundamental and the doubled frequency of the laser field (2). The values $\Delta_{\omega}^{(1)}$ and $\Delta_{\gamma}^{(1)}$ are nonzero due to an asymmetry of the states $|2\rangle$ and $|3\rangle$ of atomic hydrogen in parabolic coordinates.

The parameters $\bar{\gamma}_{\text{tr}}$, $\Delta_{\gamma}^{(1)}$, and $\Delta_{\gamma}^{(2)}$ of the decoherence rate for each combination of intensity and wavelength of the IR field were determined via *ab initio* solution of an independent auxiliary problem. For this purpose, TDSE was solved for an atom initially put into the resonant excited state and subjected to the IR field of required intensity and wavelength. Then, the norm of electron wave function in the vicinity of the atomic core (inside a sphere with radius $R = 25$ atomic units) was calculated numerically. As a result, the probability for an atom to remain nonionized by the IR field was found as a function
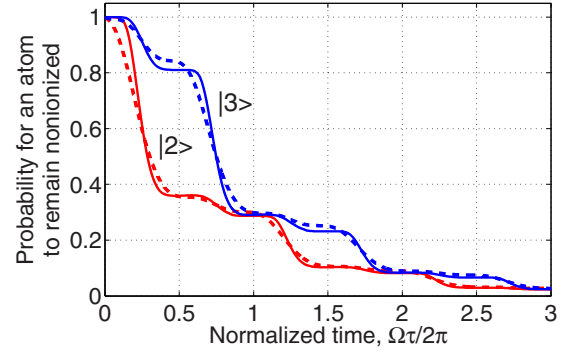

FIG. 1. Time dependencies of a probability for a hydrogen atom initially excited into the state $|2\rangle$ or $|3\rangle$ to remain nonionized by the monochromatic IR field of intensity $I_{\text{IR}} = 2.5 \times 10^{12}$ W/cm² and wavelength $\lambda_{\text{IR}} = 8\,\mu\text{m}$. The lower red curves correspond to the state $|2\rangle$, while the upper blue curves characterize the state $|3\rangle$. The solid curves are the results of *ab initio* solution of the TDSE, whereas the dashed curves represent the approximation (10b).

of time. An example of such a calculation is shown in Fig. 1. The parameters $\bar{\gamma}_{\text{tr}}$, $\Delta_{\gamma}^{(1)}$, and $\Delta_{\gamma}^{(2)}$ were then found via fitting the obtained time dependence by $\exp\{\int_0^\tau \gamma_{s1}(\tau')d\tau'\}$, where $\gamma_{s1}(\tau')$ is given by Eq. (10b). The amplitude of the linear Stark effect, $\Delta_{\omega}^{(1)}$, is calculated via the perturbation theory: $\Delta_{\omega}^{(1)} = \frac{3\hbar}{m_e e} E_C$ (m_e is the electron mass); the time-averaged transition frequency is $\bar{\omega}_{\text{tr}} = \omega_{21}^{(0)} - \Delta_{\omega}^{(2)}$; finally, the amplitude of the quadratic Stark shift, $\Delta_{\omega}^{(2)}$, is chosen to provide the best agreement between the generalized analytical solution and the results of TDSE calculations for the output XUV radiation. In the limit of low-frequency and low-intensity modulating IR field, the values of $\Delta_{\omega}^{(2)}$ determined in this way are comparable to those predicted by the perturbation theory. Thus, for a 10.65-μm IR field with intensity 1.4×10^{12} W/cm², we get $\Delta_{\omega}^{(2)} = 0.46\Omega$, while the static perturbation theory gives $\Delta_{\omega}^{(2)} = 0.52\Omega$. In the case of stronger and higher-frequency IR fields, the perturbation theory overestimates the quadratic Stark shift.

The steady-state solution of Eqs. (7)–(10) reads

$$\tilde{E}_{\text{Scatt}}(L,\tau) = -E_0 L \frac{2\pi N d_{\text{tr}}^2 \omega_0}{\hbar c} \exp\left\{\left(i P_{\omega}^{(2)} - P_{\gamma}^{(2)}\right)\sin(2\Omega\tau)\right\}$$

$$\times \sum_{n,l,m,k=-\infty}^{\infty} (i)^{m+k} J_n\left(P_{\omega}^{(1)}\right) J_l\left(P_{\omega}^{(2)}\right) I_m\left(P_{\gamma}^{(1)}\right) I_k\left(P_{\gamma}^{(2)}\right) \exp\left\{-i2(l+k)\Omega\tau\right\}$$

$$\times \left[\frac{\exp\left\{\left(i P_{\omega}^{(1)} - P_{\gamma}^{(1)}\right)\sin(\Omega\tau) - i(n+m)\Omega\tau\right\}}{i(\bar{\omega}_{\text{tr}} - \omega_0 - [(n+m)+2(l+k)]\Omega) + \bar{\gamma}_{\text{tr}}} + \frac{\exp\left\{-\left(i P_{\omega}^{(1)} - P_{\gamma}^{(1)}\right)\sin(\Omega\tau) + i(n+m)\Omega\tau\right\}}{i\{\bar{\omega}_{\text{tr}} - \omega_0 + [(n+m) - 2(l+k)]\Omega\} + \bar{\gamma}_{\text{tr}}}\right], \quad (11)$$

where $J_k(x)$ and $I_k(x)$ are the Bessel function of the first kind and the modified Bessel function of order k, respectively, and $P_{\omega}^{(1)} \equiv \frac{\Delta_{\omega}^{(1)}}{\Omega}$, $P_{\gamma}^{(1)} \equiv \frac{\Delta_{\gamma}^{(1)}}{\Omega}$, $P_{\omega}^{(2)} \equiv \frac{\Delta_{\omega}^{(2)}}{2\Omega}$, $P_{\gamma}^{(2)} \equiv \frac{\Delta_{\gamma}^{(2)}}{2\Omega}$ are the modulation indices.

The Fourier decomposition of the resonantly scattered radiation (11) has a form

$$\tilde{E}_{\text{Scatt}}(L,\tau) = -E_0 L \frac{2\pi N d_{\text{tr}}^2 \omega_0}{\hbar c} \sum_{\substack{n,l,m,k,\\g,s,p,f=-\infty}}^{\infty} (i)^{m+k+s+f} J_n\big(P_\omega^{(1)}\big) J_l\big(P_\omega^{(2)}\big) J_p\big(P_\omega^{(2)}\big) I_m\big(P_\gamma^{(1)}\big) I_s\big(P_\gamma^{(1)}\big) I_k\big(P_\gamma^{(1)}\big) I_f\big(P_\gamma^{(2)}\big)$$

$$\times \left[\frac{J_{(n+m)+2(l+k)-2(p+f)-(g+s)}\big(P_\omega^{(1)}\big)}{i\{\bar{\omega}_{\text{tr}} - \omega_0 - [(n+m)+2(l+k)]\Omega\} + \bar{\gamma}_{\text{tr}}} + \frac{J_{(n+m)-2(l+k)+2(p+f)+(g-s)}\big(P_\omega^{(1)}\big)}{i\{\bar{\omega}_{\text{tr}} - \omega_0 + [(n+m)-2(l+k)]\Omega\} + \bar{\gamma}_{\text{tr}}} \right] \exp\{-ig\Omega\tau\}.$$

(12)

As mentioned above, along with the generalized solution (7), (11), and (12), the results of TDSE calculations are compared to the simplified analytics derived previously [36] within the approximations $P_\omega^{(2)} = P_\gamma^{(1)} = P_\gamma^{(2)} = 0$, $\bar{\gamma}_{\text{tr}} \ll \Omega$, and $\omega_0 = \bar{\omega}_{\text{tr}} + m_* \Omega$, where $m_* = 0, \pm 1, \pm 2, \ldots$:

$$\tilde{E}_{\text{Scatt}}(L,\tau) = -E_0 L J_{m_*}\big(P_\omega^{(1)}\big) \frac{4\pi N d_{\text{tr}}^2 \omega_0}{\hbar c \bar{\gamma}_{\text{tr}}} \exp\{im_*\Omega t\} \times \begin{cases} \sum_{n=-\infty}^{+\infty} J_{2n}\big(P_\omega^{(1)}\big) \exp\{-i2n\Omega t\}, & m_* = 2k \\ \sum_{n=-\infty}^{+\infty} J_{2n+1}\big(P_\omega^{(1)}\big) \exp\{-i(2n+1)\Omega t\}, & m_* = 2k+1 \end{cases}. \quad (13)$$

Due to its simplicity, the analytical solution (13) allows us to determine the optimal conditions for ultrashort pulse formation via the linear Stark effect in atomic hydrogen. As shown in [36], the output XUV radiation represents a train of bandwidth-limited pulses if (i) the incident radiation is tuned to the time-averaged position of the atomic resonance, $\omega_0 = \bar{\omega}_{\text{tr}}$; (ii) the modulation index $P_\omega^{(1)}$ satisfies the inequality $\nu_0^{(1)} < P_\omega^{(1)} < \nu_2^{(1)}$, where $\nu_0^{(1)} \cong 2.40$ is the first root of equation $J_0(\nu) = 0$ and $\nu_2^{(1)} \cong 5.14$ is the first root of equation $J_2(\nu) = 0$; and (iii) the resonant component of the output XUV radiation is attenuated to the level of the generated sidebands. In Figs. 2–5 we compare the results of both the generalized, (11) and (12), and the simplified, (13), analytical solutions to the *ab initio* solutions of the TDSE under these optimal conditions for different combinations of intensity, I_{IR}, and wavelength, λ_{IR}, of the IR field (2). The analytically calculated envelope, (7) and (11), of the output XUV radiation is slightly shifted along the time axis in order to provide the best fit to the numerical results. This shift originates from inertia of electronic response to the IR field. The timing of pulses predicted by the analytical solution is fully determined by time dependencies of frequencies and decoherence rates of the resonant transitions $|1\rangle \leftrightarrow |2\rangle$ and $|1\rangle \leftrightarrow |3\rangle$. Equations (10a) and (10b) assume that both the frequencies and the decoherence rates reach their maximum values at maxima of absolute value of the IR field strength. This is correct for the linear Stark shifts but not exactly correct for the decoherence rates. The resonant interaction between the atoms and the XUV field decreases with decrease of an overlap between the wave functions of the atomic ground state and of the ionized electron. Therefore, the peak of the decoherence rate is slightly delayed with respect to the peak of the excited-state ionization rate (and the peak of IR field strength) by a time interval needed for the electron to move away from the nucleus by a distance equal to the average radius of its wave function (which can be estimated on the basis of initial wave function of the resonant excited state). In such a case, if there were no Stark effect, the results of *ab initio* solution for the time dependence of the output XUV intensity would be delayed with respect to the analytical solution by this time interval,

which is not taken into account by Eq. (10b) but naturally arises in numerical TDSE solution. However, as far as the IR field intensity is below the threshold of rapid excited-state ionization, the pulse shape is predominantly determined by the linear Stark effect, which is instantaneous. For this reason, in the case of low-intensity IR fields, the temporal shift, τ_0, between the analytical and numerical solutions for the output XUV intensity which maximizes their overlap, is very small ($\sim 10^{-3}$ of the IR field cycle). With increasing intensity and frequency of the IR field, the value of τ_0 increases to $\sim 10^{-2}$ of the IR field cycle. In the TDSE calculations, we assume the IR field in the form $E_{\text{IR}}(\tau) = E_C(\tau)\sin(\Omega\tau)$, with the slowly varying amplitude $E_C(\tau) = \sin^2(\Omega\tau/40)$ for $0 \leqslant \tau \leqslant 20\pi/\Omega$ and $E_C(\tau) = 1$ for $20\pi/\Omega < \tau \leqslant 230\pi/\Omega$. The XUV radiation has the form $E_{\text{XUV}}(\tau) = \tilde{E}_{\text{XUV}}(\tau)\sin[\omega_0(\tau - \tau_0)]$, where $\tau_0 = 30\pi/\Omega$ and $\tilde{E}_{\text{XUV}}(\tau) \equiv 0$ for $0 \leqslant \tau \leqslant 30\pi/\Omega$, $\tilde{E}_{\text{XUV}}(\tau) = \sin^2[\Omega(\tau - \tau_0)/20]$ for $30\pi/\Omega < \tau \leqslant 40\pi/\Omega$, $\tilde{E}_{\text{XUV}}(\tau) = 1$ for $40\pi/\Omega < \tau \leqslant 220\pi/\Omega$, and $\tilde{E}_{\text{XUV}}(\tau) = \cos^2[\Omega(\tau - 220\pi/\Omega)/20]$ for $220\pi/\Omega < \tau \leqslant 230\pi/\Omega$. For each combination of intensity and wavelength of the IR field, the wavelength of XUV radiation, λ_{XUV}, is adjusted to the Stark-shifted position of the atomic resonance.

In Fig. 2, we present the results for atomic hydrogen irradiated by the CO_2-laser field with intensity $I_{\text{IR}} = 1.4 \times 10^{12}$ W/cm^2 and wavelength $\lambda_{\text{IR}} = 10.65\,\mu$m, corresponding to the modulation index value $P_\omega^{(1)} = 4.45$. These are exactly the same parameters as in the original paper [36]. The medium is simultaneously irradiated by the XUV radiation with wavelength $\lambda_{\text{XUV}} = 122.2$ nm and intensity $I_{\text{XUV}} = 2.2 \times 10^8$ W/cm^2, resonantly exciting the atomic transition $n = 1 \leftrightarrow n = 2$. As seen from this figure (whose panels (a) and (b) are remarkably similar to Figs. 3 and 4 of [36]), the *ab initio* TDSE solution fully confirms the possibility of pulse train formation. The pulses produced in this case are bandwidth limited and have the duration $\tau_{\text{pulse}} = 2.7$ fs and repetition period $T = 17.8$ fs. The analytical solutions (11)–(13) are in excellent agreement with each other and with the *ab initio* TDSE solution both in time- and frequency-domain representations; see Figs. 2(a) and 2(b), respectively. This is what we should actually expect, since for such parameters of the IR
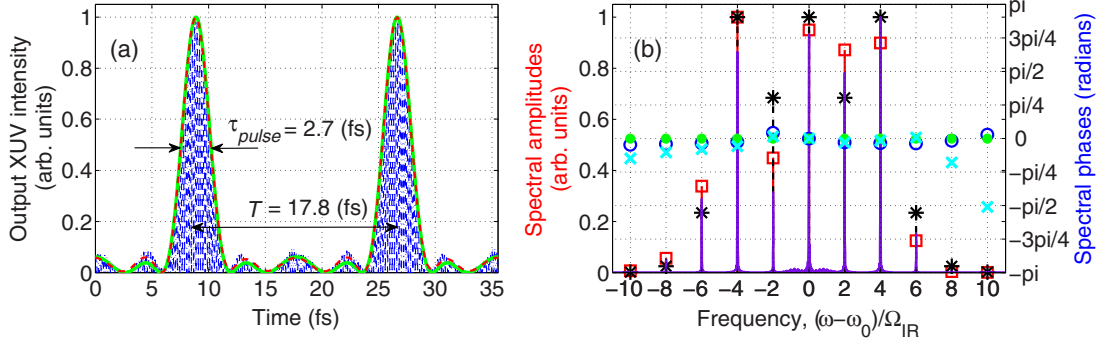
FIG. 2. (a) Time dependence of intensity $I \sim |\tilde{E}_{\mathrm{XUV}}|^2$ of XUV radiation at the exit of an optically thin medium of atomic hydrogen simultaneously irradiated by the CO_2-laser field with intensity $I_{\mathrm{IR}} = 1.4 \times 10^{12}\,\mathrm{W/cm^2}$ and wavelength $\lambda_{\mathrm{IR}} = 10.65\,\mu\mathrm{m}$ and the XUV radiation with intensity $I_{\mathrm{XUV}} = 2.2 \times 10^8\,\mathrm{W/cm^2}$ and wavelength $\lambda_{\mathrm{XUV}} = 122.2\,\mathrm{nm}$. The dimensionless parameters in analytical solution are $P_\omega^{(1)} = 4.45$, $P_\omega^{(2)} = 0.23$, $P_\gamma^{(1)} = 0.05$, $P_\gamma^{(2)} = 0.015$, and $\bar{\gamma}_{\mathrm{tr}} = 0.04\Omega$. The dashed red curve and the solid green curve correspond to the analytical solutions (11) and (13), respectively. The rapidly oscillating dash-dotted blue curve shows the numerical solution of the TDSE for the squared value of the XUV field strength, $|E_{\mathrm{XUV}}|^2$. (b) Fourier transform of the output XUV radiation corresponding to the time dependence in (a). The results provided by the generalized analytical solution (12) for the amplitudes and phases of the spectral components are shown by red squares and blue circles, while the predictions of the simplified analytical theory (13) for the spectral amplitudes and phases are plotted by black asterisks and filled green circles. The lavender curve and cyan crosses show the *ab initio* solution of the TDSE for the amplitudes of the spectral components, as well as their phases at the combinational frequencies, $\omega = \omega_0 + n\Omega$, $n = 0, \pm 1, \pm 2, \ldots$, respectively. The resonant spectral component, $\omega = \omega_0$, of the output XUV radiation is attenuated to the level of the generated sidebands.

field the applicability conditions of Eq. (13) are well satisfied: (i) the spectral lines of the resonant transitions are narrow with respect to the laser frequency due to the very low excited-state ionization rates; (ii) the sub-laser-cycle oscillations of the quadratic Stark shift and the ionization rates are not important, since their amplitudes are small compared to both the laser frequency and the amplitude of linear Stark splitting; and (iii) for the considered values of frequency and intensity of the IR field, the nonadiabatic effects are negligible.

The duration of the bandwidth-limited pulses is inversely proportional to their bandwidth. Therefore, according to (13), for a fixed value of modulation index $P_\omega^{(1)}$ the pulse duration (as well as the repetition period) is inversely proportional to the frequency of the IR field and proportional to its wavelength, $\tau_{\mathrm{pulse}} \sim \Omega^{-1} \sim \lambda_{\mathrm{IR}}$. Let us further examine the possibilities to shorten the pulses via the reduction of the wavelength of the IR field. In the following, we consider the cases of $\lambda_{\mathrm{IR}} = 8, 4$, and $2\,\mu\mathrm{m}$. In order to keep the modulation

index constant, $P_\omega^{(1)} = 4.45$, the intensity of the IR field is chosen to increase inversely proportional to the square of its wavelength, $I_{\mathrm{IR}} \sim \lambda_{\mathrm{IR}}^{-2}$. Figures 3 and 4 correspond to the IR field with wavelength $\lambda_{\mathrm{IR}} = 8$ and $4\,\mu\mathrm{m}$ and intensity $I_{\mathrm{IR}} = 2.5 \times 10^{12}$ and $10^{13}\,\mathrm{W/cm^2}$, respectively. Due to increasing time-averaged quadratic Stark shift of the excited energy levels $|2\rangle$ and $|3\rangle$, the wavelength of the resonant XUV radiation grows with increasing intensity of the IR field. For instance, we have $\lambda_{\mathrm{XUV}} = 122.6\,\mathrm{nm}$ for the 8-$\mu\mathrm{m}$ IR field and $\lambda_{\mathrm{XUV}} = 124.6\,\mathrm{nm}$ for the 4-$\mu\mathrm{m}$ IR field. The intensity of XUV radiation is $I_{\mathrm{XUV}} = 1.6 \times 10^9$ and $10^9\,\mathrm{W/cm^2}$, respectively (it should be much lower than the intensity of the modulating field and much higher than the intensity of its high-order harmonics). In both cases, a train of pulses is produced at the exit of the medium. It is worth noting that we regard the parameter values as suitable for the pulse formation if the peak intensity of spikes in between the pulses does not exceed half peak intensity of the pulses. Certainly, the "suitability"
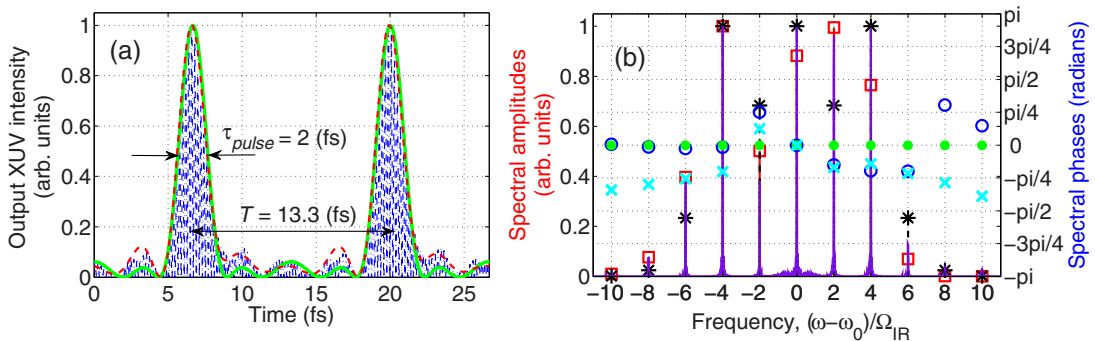

FIG. 3. (a) Same as Fig. 2(a), but for IR field with intensity $I_{\mathrm{IR}} = 2.5 \times 10^{12}\,\mathrm{W/cm^2}$ and wavelength $\lambda_{\mathrm{IR}} = 8\,\mu\mathrm{m}$, and XUV radiation with intensity $I_{\mathrm{XUV}} = 1.6 \times 10^9\,\mathrm{W/cm^2}$ and wavelength $\lambda_{\mathrm{XUV}} = 122.6\,\mathrm{nm}$. The dimensionless parameters in analytical solutions are $P_\omega^{(1)} = 4.45$, $P_\omega^{(2)} = 0.32$, $P_\gamma^{(1)} = 0.21$, $P_\gamma^{(2)} = 0.074$, and $\bar{\gamma}_{\mathrm{tr}} = 0.19\Omega$. (b) Fourier transform of the output XUV radiation corresponding to the time dependence in (a). Designations are the same as in Fig. 2(b).
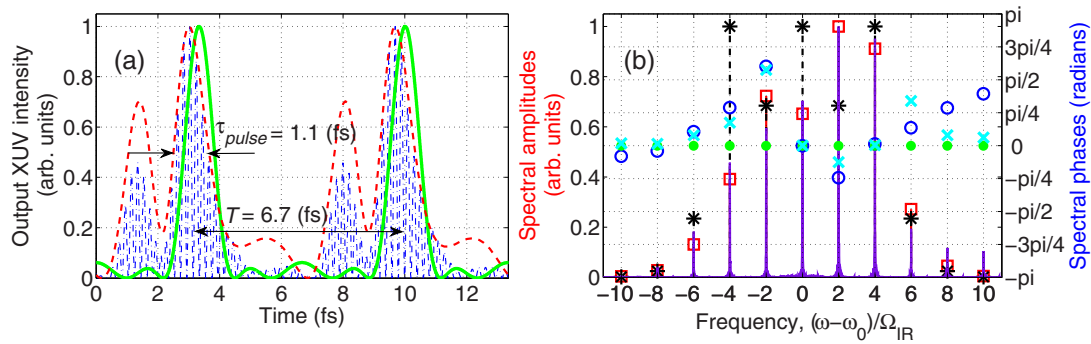
FIG. 4. (a) Same as Fig. 2(a), but for IR field with intensity $I_{IR} = 10^{13}$ W/cm^2 and wavelength $\lambda_{IR} = 4\,\mu$m, and XUV radiation with intensity $I_{XUV} = 10^9$ W/cm^2 and wavelength $\lambda_{XUV} = 124.6$ nm. The dimensionless parameters in analytical solutions are $P_\omega^{(1)} = 4.45$, $P_\omega^{(2)} = 0.23$, $P_\gamma^{(1)} = 0.8$, $P_\gamma^{(2)} = 0.6$, and $\bar{\gamma}_{tr} = 1.3\Omega$. (b) Fourier transform of the output XUV radiation corresponding to the time dependence in (a). Designations are the same as in Fig. 2(b).

criterion can be defined in different ways depending on the application of the pulses which one keeps in mind. In the case of the 8-μm IR field, Fig. 3, the duration of pulses equals $\tau_{pulse} = 2$ fs and the repetition period is $T = 13.3$ fs, while for the 4-μm IR field, Fig. 4, the pulse duration and repetition period are $\tau_{pulse} = 1.1$ fs (which corresponds to 2.6 cycles of the carrier) and $T = 6.7$ fs, respectively. Accordingly, the *ab initio* calculation results show the possibility of producing nearly 1-fs few-cycle pulses via the linear Stark effect in atomic hydrogen (reducing the ultimate pulse duration by a factor of more than 2 compared to the results of [36]) using IR fields with wavelength $\geqslant 4\,\mu$m. It is noteworthy that at the cost of reducing the ratio of pulse repetition period to the pulse duration, one is able to use a shorter wavelength IR field of intensity $I_{IR} \leqslant 10^{13}$ W/cm^2, corresponding to $P_\omega^{(1)} > 2.4$, for the pulse formation. Experimentally, such an IR field can be produced by an OPCPA laser system [50], while the resonant XUV radiation can be generated via nonlinear upconversion of a visible laser field [51,52]. Further reduction of the pulse duration can be achieved via the linear Stark effect in hydrogenlike ions [31,36]. As follows from similarity between the hydrogenlike ions, using the ions with nucleus charge $-eZ$, reducing the wavelengths of both the XUV radiation and the IR field by a factor of Z^2, and increasing the intensity of the IR field by a factor of Z^6 with respect to the case of atomic hydrogen will result in the formation of pulses with Z^2 times shorter duration and repetition period. In particular, in the case of Li^{2+} ions, $Z = 3$, exposed to the XUV radiation with wavelength $\lambda_{XUV} = 13.84$ nm and the IR field with wavelength $\lambda_{IR} = 440$ nm and intensity $I_{IR} = 7.3 \times 10^{15}$ W/cm^2, a train of pulses will be produced with the same shape as in Fig. 4(a) but with the pulse duration $\tau_{pulse} = 120$ as and repetition period $T = 730$ as.

With decreasing wavelength and increasing intensity of the IR field, the results of *ab initio* calculations for atomic hydrogen increasingly deviate from the predictions of the simplified analytical theory (13); see Figs. 2–4. However, these deviations are basically reproduced by the generalized analytical solution (11). Thus, they can be attributed to (i) ionization broadening of the resonant transition lines, as well as (ii) sub-laser-cycle oscillations of both the quadratic Stark shift of the excited

energy levels and ionization rates from them. The generalized analytics shows that in the cases of 8- and 4-μm IR fields, the distortions of the pulse shape predominantly originate from the time-independent part of the excited-state ionization rate, causing broadening of the resonant transition lines and violation of the inequality $\bar{\gamma}_{tr} \ll \Omega$. In the case of shorter wavelength, $\lambda_{IR} = 2\,\mu$m, and, respectively, higher intensity, $I_{IR} = 4 \times 10^{13}$ W/cm^2, of the IR field, which is addressed in Fig. 5 (the corresponding wavelength of the resonant XUV radiation is $\lambda_{XUV} = 133.4$ nm; the XUV intensity is chosen to be $I_{XUV} = 4 \times 10^9$ W/cm^2), sub-laser-cycle oscillations of ionization rate become quite important. As shown in [37], rapid quasistatic ionization (which depopulates the resonant excited state within each half cycle of the IR field) itself leads to the transformation of XUV radiation into few-cycle pulses due to the periodic switching of its resonant interaction with atoms on and off twice within the IR field cycle. The intensity of the IR field assumed in Fig. 5 is not yet enough for such an ionization switching to occur. However, the peak excited-state ionization rate already exceeds the amplitude of the linear Stark effect, so that the simplified analytical solution (13) is not yet applicable, and the two mechanisms of pulse formation compete with each other, leading to beatings in the time dependence of the output XUV intensity; see Fig. 5(a). At the same time, the generalized analytical solution (11) and (12) remains valid in this case, being in qualitative agreement with the results of *ab initio* solution both in time domain, Fig. 5(a), and frequency domain, Fig. 5(b).

In summary, the *ab initio* calculations show that intensities of the IR field suitable for the ultrashort or few-cycle pulse formation via the linear Stark effect are limited by the values at which atomic ionization from the resonant excited state becomes significant. Further increase of intensity of the IR field leads to the dominating effect of the excited-state ionization on the resonant atomic response and provides the conditions for the few-cycle pulse formation due to the ionization-switching mechanism [37]. As was previously shown, the ionization switching can be implemented in arbitrary atomic gas. In the following section, we consider this regime of pulse formation in helium, which is more convenient for an experimental implementation compared to atomic hydrogen.
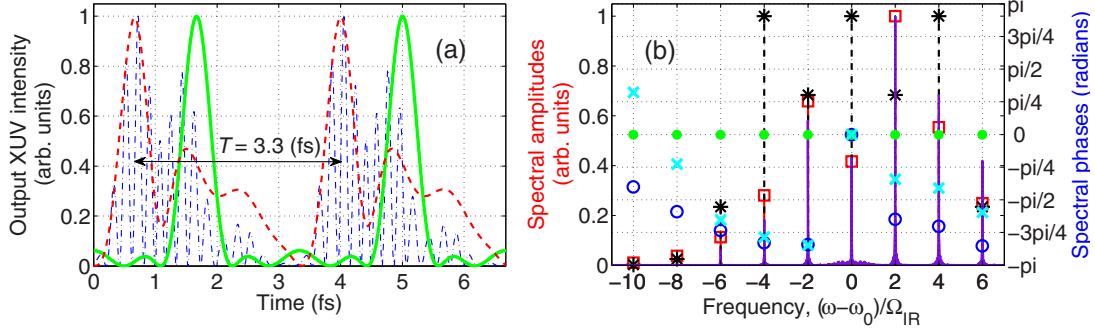
FIG. 5. (a) Same as Fig. 2(a), but for IR field with intensity $I_{IR} = 4 \times 10^{13}$ W/cm^2 and wavelength $\lambda_{IR} = 2\,\mu$m, and XUV radiation with intensity $I_{XUV} = 4 \times 10^9$ W/cm^2 and wavelength $\lambda_{XUV} = 133.4$ nm. The dimensionless parameters in analytical solutions are $P_\omega^{(1)} = 4.45$, $P_\omega^{(2)} = 0.5$, $P_\gamma^{(1)} = 1.9$, $P_\gamma^{(2)} = 1.8$, and $\bar{\gamma}_{tr} = 3.8\Omega$. (b) Fourier transform of the output XUV radiation corresponding to the time dependence in (a). Designations are the same as in Fig. 2(b).

III. ATTOSECOND PULSE FORMATION VIA EXCITED-STATE IONIZATION IN HELIUM

In the case of helium, we use the unperturbed atomic Hamiltonian from [53], which provides a relatively good description of the lowest excited states of He in the single-active-electron approximation.

The incident XUV radiation is tuned in resonance with the unperturbed atomic transition $1s^2 \leftrightarrow 1s2p$. As shown in [37], this choice of frequency of the XUV radiation is optimal for attosecond pulse formation via ionization switching of its resonant interaction with the atoms: The interaction is switched on in the vicinity of zero crossings of the IR field strength, when the atomic transition is nearly unperturbed, and switched off the rest of the time, when the transition line is strongly broadened due to rapid excited-state ionization. Similarly to the case of hydrogen, in order to analyze the results of *ab initio* calculations, we derive the generalized analytical theory taking into account space-time dependencies of both the Stark effect and excited-state ionization. However, in the case of helium, it is considerably simpler: since the energy level $1s2p$ is nondegenerate, the resonant atomic response is correctly described within the two-level approximation, in which the lower and upper energy levels correspond to the states $|1\rangle = 1s^2$ and $|2\rangle = 1s2p$, respectively. In such a case, the slowly varying amplitude of the atomic polarization is given by

$$\tilde{P}(\tau) = 2N d_{tr} a_{21}(\tau), \tag{14}$$

and the amplitude of the atomic coherence satisfies the equation

$$\frac{da_{21}}{d\tau} + \{i[\omega_{21}(\tau) - \omega_0] + \gamma_{21}(\tau)\}a_{21} = i\frac{d_{tr}E_0}{2\hbar}. \tag{15}$$

Since both $|1\rangle$ and $|2\rangle$ states possess a central symmetry, the simplest approximation for the time dependencies of the instantaneous frequency, $\omega_{21}(\tau)$, and decoherence rate, $\gamma_{21}(\tau)$, of the resonant transition is harmonic:

$$\omega_{21}(\tau) = \bar{\omega}_{tr} + \Delta_\omega^{(2)} \cos(2\Omega\tau), \tag{16a}$$

$$\gamma_{21}(\tau) = \bar{\gamma}_{tr} + \Delta_\gamma^{(2)} \cos(2\Omega\tau), \tag{16b}$$

where $\bar{\omega}_{tr} = \omega_{21}^0 + \Delta_\omega^{(2)}$ and $\bar{\gamma}_{tr} = \gamma_{21}^0 + \Delta_\gamma^{(2)}$. Similarly to the case of atomic hydrogen, for each combination of intensity and wavelength of the IR field, the values γ_{21}^0 and $\Delta_\omega^{(2)}$ are found via fitting to the results of the auxiliary TDSE calculation for the time dependence of the probability for an atom, which was initially excited into the state $|2\rangle$ and exposed to the IR field, to remain nonionized. The fitting gives $\gamma_{21}^0 = 0$ in all the cases. The amplitude of the quadratic Stark effect, $\Delta_\omega^{(2)}$, is chosen to provide the best agreement between the time dependencies of the output XUV intensity calculated analytically and numerically. The obtained values of $\Delta_\omega^{(2)}$ are comparable to the values of $\Delta_\gamma^{(2)}$ and are much smaller than those predicted by the perturbation theory, similar to what has been obtained in the previous studies of Stark effect in strong fields [54,55].

The steady-state solution of Eqs. (7) and (14)–(16) has the form

$$\tilde{E}_{Scatt}(L, \tau) = -E_0 L \frac{2\pi N d_{tr}^2 \omega_0}{\hbar c} \times \exp\left\{-\left(i P_\omega^{(2)} + P_\gamma^{(2)}\right)\sin(2\Omega\tau)\right\} \sum_{k,m=-\infty}^{\infty} (i)^m J_{k+m}\left(P_\omega^{(2)}\right) I_m\left(P_\gamma^{(2)}\right) \frac{\exp\{i2k\Omega\tau\}}{i(\bar{\omega}_{tr} - \omega_0 + 2k\Omega) + \bar{\gamma}_{tr}}, \tag{17}$$

where $P_\omega^{(2)} \equiv \Delta_\omega^{(2)}/2\Omega$ and $P_\gamma^{(2)} \equiv \Delta_\gamma^{(2)}/2\Omega$.

The Fourier decomposition of (17) is

$$\tilde{E}_{Scatt}(L, \tau) = -E_0 L \frac{2\pi N d_{tr}^2 \omega_0}{\hbar c} \sum_{k,n,l,m=-\infty}^{\infty} (i)^{l+m} J_{n+m-l-k}\left(P_\omega^{(2)}\right) J_n\left(P_\omega^{(2)}\right) I_l\left(P_\gamma^{(2)}\right) I_m\left(P_\gamma^{(2)}\right) \frac{\exp\{i2k\Omega\tau\}}{i[\bar{\omega}_{tr} - \omega_0 + 2(n-l)\Omega] + \bar{\gamma}_{tr}}. \tag{18}$$

Along with the generalized analytical solution (17) and (18), the results of TDSE calculations for helium are compared to the previously derived solution [37], which neglects the Stark effect by assuming $\omega_{21}(\tau) = \bar{\omega}_{tr}$ and assumes a stepwise temporal change of the excited-state ionization rate:

$$\gamma_{21}(\tau) = \begin{cases} \bar{\gamma}_{\min}, & 0 \leqslant \tau < \Delta t_{zero} \\ \bar{\gamma}_{\max}, & \Delta t_{zero} \leqslant \tau < \pi/\Omega \end{cases}, \quad \gamma_{21}(\tau + \pi/\Omega) = \gamma_{21}(\tau). \tag{19}$$

The decoherence rate (19) possesses a half-IR-field-cycle periodicity, taking the minimum value, $\bar{\gamma}_{\min}$, near a zero crossing of the IR field at $\tau = \Delta t_{zero}/2$ (which corresponds to $\varphi_0 = [\pi - \Omega \Delta t_{zero}]/2$ in Eq. (2)) and the maximum value, $\bar{\gamma}_{\max}$, the rest of the time. In order to find the values $\bar{\gamma}_{\min}$, $\bar{\gamma}_{\max}$, and Δt_{zero} for each combination of intensity and wavelength of the IR field, we perform the following steps: first, we find the ratio $\bar{\gamma}_{\max}/\bar{\gamma}_{\min}$ using the nonadiabatic tunneling ionization rate [56] and calculate the time-averaged decoherence rate

$\bar{\gamma}_{av} \equiv \frac{\Omega}{\pi}[\bar{\gamma}_{\min}\Delta t_{zero} + \bar{\gamma}_{\max}(\frac{\pi}{\Omega} - \Delta t_{zero})]$. Then, we use the exponential function $\exp(-2\bar{\gamma}_{av}\tau)$ for fitting to the results of auxiliary TDSE calculation for the time dependence of the probability for an atom in the state $|2\rangle$ to remain nonionized under the action of the IR field. These steps allow us to represent $\bar{\gamma}_{\min}$ and $\bar{\gamma}_{\max}$ as $\bar{\gamma}_{\min} = \bar{\gamma}_{\min}(\Delta t_{zero})$ and $\bar{\gamma}_{\max} = \bar{\gamma}_{\max}(\Delta t_{zero})$, respectively. Finally, we choose Δt_{zero} to provide best agreement between the analytical and numerical results for the time dependence of the output XUV intensity.

In such an approximation, the slowly varying amplitude of the resonantly scattered XUV radiation takes the form

$$\tilde{E}_{Scatt}(\tau) = \begin{cases} \tilde{E}_{Scatt}^{(1)}(\tau), & 0 \leqslant \tau < \Delta t_{zero} \\ \tilde{E}_{Scatt}^{(2)}(\tau), & \Delta t_{zero} \leqslant \tau < \pi/\Omega \end{cases}, \quad \tilde{E}_{Scatt}(\tau + \pi/\Omega) = \tilde{E}_{Scatt}(\tau), \tag{20}$$

$$\tilde{E}_{Scatt}^{(1)}(\tau) = \tilde{C}_1 \exp\{(i\,\Delta\omega - \bar{\gamma}_{\min})\tau\} + \tilde{D}_1,$$
$$\tilde{E}_{Scatt}^{(2)}(\tau) = \tilde{C}_2 \exp\{(i\,\Delta\omega - \bar{\gamma}_{\max})(\tau - \Delta t_{zero})\} + \tilde{D}_2, \tag{21}$$

where $\Delta\omega \equiv \omega_0 - \bar{\omega}_{tr}$. The coefficients $\tilde{C}_1$, $\tilde{C}_2$ and $\tilde{D}_1$, $\tilde{D}_2$, in their turn, have the form

$$\tilde{D}_1 = -E_0 L \frac{2\pi N d_{tr}^2 \omega_0}{\hbar c(\bar{\gamma}_{\min} - i\,\Delta\omega)}, \quad \tilde{D}_2 = -E_0 L \frac{2\pi N d_{tr}^2 \omega_0}{\hbar c(\bar{\gamma}_{\max} - i\,\Delta\omega)}, \tag{22}$$

$$\tilde{C}_1 = (\tilde{D}_2 - \tilde{D}_1)\frac{\exp\{(i\,\Delta\omega - \bar{\gamma}_{\max})(\pi/\Omega - \Delta t_{zero})\} - 1}{\exp\{(i\,\Delta\omega - \bar{\gamma}_{\max})\pi/\Omega\}\exp\{(\bar{\gamma}_{\max} - \bar{\gamma}_{\min})\Delta t_{zero}\} - 1},$$

$$\tilde{C}_2 = (\tilde{D}_1 - \tilde{D}_2)\frac{\exp\{(i\,\Delta\omega - \bar{\gamma}_{\min})\Delta t_{zero}\} - 1}{\exp\{(i\,\Delta\omega - \bar{\gamma}_{\max})\pi/\Omega\}\exp\{(\bar{\gamma}_{\max} - \bar{\gamma}_{\min})\Delta t_{zero}\} - 1}. \tag{23}$$

An analytical expression for the Fourier transform of the solution (20)–(23) for the resonantly scattered radiation is given in [37].

In the regime of rapid excited-state ionization, which depopulates the resonant excited atomic state twice per IR-field cycle, the generated XUV sidebands are in antiphase with the incident XUV radiation and in phase with each other, which corresponds to confinement of the resonant absorption of the XUV radiation within extremely short time intervals near zero crossings of the IR field [37]. In such a case, the resonantly scattered XUV radiation (17), or (20)–(23), itself represents a train of few-cycle pulses. Therefore, the generation of attosecond pulses at the output of the medium can be achieved via suppression of the central spectral component of XUV radiation (at the frequency of the incident field), for example, via its resonant absorption in an additional layer of helium, which is not modulated by the IR field.

The results provided by both analytical solutions (17) and (18), and (20)–(23), are compared in Figs. 6–10 to the *ab initio* TDSE calculations for the helium. Timing of the analytically calculated envelopes of the output XUV radiation is fitted to the numerical solutions within a few percent of the laser cycle. Similarly to the case of atomic hydrogen, this time shifting originates from inertia of atomic response to the IR field: The ionized electron continues to participate in the intra-atomic processes while its wave function overlaps with the atomic ground state. The TDSE calculations presented in this section imply the IR field in the form $E_{IR}(\tau) = E_C(\tau)\sin(\Omega\tau)$, with $E_C(\tau) = \sin^2(\Omega\tau/40)$ for $0 \leqslant \tau \leqslant 20\pi/\Omega$ and $E_C(\tau) = 1$ for $20\pi/\Omega < \tau \leqslant 90\pi/\Omega$. The XUV radiation has the form $E_{XUV}(\tau) = \tilde{E}_{XUV}(\tau)\sin[\omega_0(\tau - \tau_0)]$, where $\tau_0 = 30\pi/\Omega$, $\tilde{E}_{XUV}(\tau) \equiv 0$ for $0 \leqslant \tau \leqslant 30\pi/\Omega$, $\tilde{E}_{XUV}(\tau) = \sin^2[\Omega(\tau - \tau_0)/20]$ for $30\pi/\Omega < \tau \leqslant 40\pi/\Omega$, $\tilde{E}_{XUV}(\tau) = 1$ for $40\pi/\Omega < \tau \leqslant 80\pi/\Omega$, and $\tilde{E}_{XUV}(\tau) = \cos^2[\Omega(\tau - 80\pi/\Omega)/20]$ for $80\pi/\Omega < \tau \leqslant 90\pi/\Omega$. The wavelength and peak intensity of the incident XUV radiation are $\lambda_{XUV} = 58.4$ nm and $I_{XUV} = 10^{11}$ W/cm^2, respectively, for all the plots.

Figure 6 represents the case of helium atoms simultaneously irradiated by the resonant XUV radiation and the IR field with
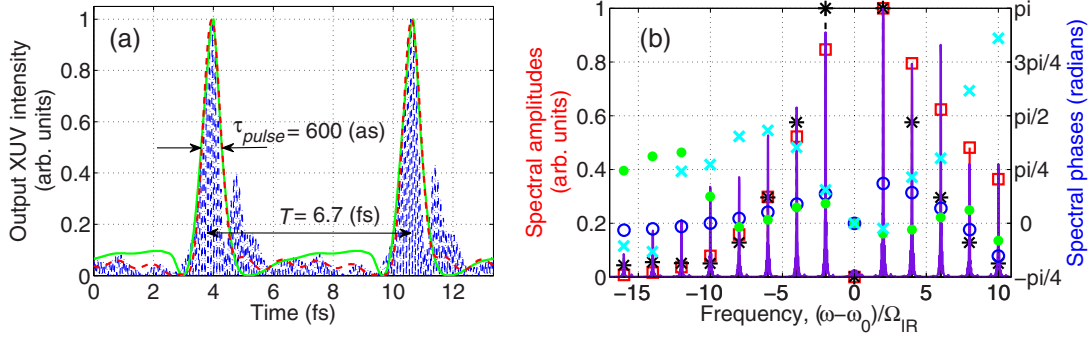
FIG. 6. (a) Time dependence of intensity of XUV radiation at the exit of an optically thin medium of helium irradiated by the IR field with intensity $I_{IR} = 1.5 \times 10^{14}$ W/cm^2 and wavelength $\lambda_{IR} = 4\,\mu$m, and the XUV radiation with intensity $I_{XUV} = 10^{11}$ W/cm^2 and wavelength $\lambda_{XUV} = 58.4$ nm. The incident spectral component of XUV radiation is suppressed. The dashed red curve and the solid green curve correspond to the harmonic and steplike analytical solutions (17), and (20)–(23), respectively. The dimensionless parameters in analytical calculations are $P_\omega^{(2)} = 15$, $P_\gamma^{(2)} = 11.5$, $\bar{\gamma}_{min}/\Omega = 0.056$, $\bar{\gamma}_{max}/\Omega = 2.7$, and $\Omega\Delta t_{zero} = 0.2\pi$. The rapidly oscillating dash-dotted blue curve is the numerical solution of the TDSE for the squared value of the XUV field strength, $|E_{XUV}|^2$. (b) Fourier transform of the output XUV radiation corresponding to the time dependence in (a). Red squares and blue circles are the amplitudes and phases of the spectral components calculated analytically via the harmonic analytical solution (18). The corresponding results of the steplike analytical solution (20)–(23) are plotted by black asterisks and green filled circles. The lavender curve and cyan crosses show the *ab initio* solution of the TDSE for the amplitudes of the spectral components, as well as their phases at the combinational frequencies, $\omega = \omega_0 + n\Omega$, $n = 0, \pm1, \pm2, \ldots$, respectively. The upper frequency limit corresponds to the ionization potential of helium.

wavelength $\lambda_{IR} = 4\,\mu$m and intensity $I_{IR} = 1.5 \times 10^{14}$ W/cm^2. After suppression of the incident spectral component, the output XUV radiation corresponds to a train of pulses with duration $\tau_{pulse} = 600$ as and repetition period $T = 6.7$ fs; see Fig. 6(a). Both analytical solutions (17), and (20)–(23), correctly describe the shape of the *main* pulse. However, the generalized analytics (17) better reproduces the pedestal. This is predominantly due to the fact that, for the assumed strength of the IR field, ionization from the resonant excited state is due to suppression of the atomic potential barrier rather than tunneling through it. In such a case, the harmonic approximation (16b) for the time dependence of the ionization rate is more suitable than the step-function model (19), which works better in the tunneling regime [57]. It is worth noting that accounting for the quadratic Stark effect in the analytical solution (17) and (18), for the resonantly scattered XUV radiation in the presence of a rapidly ionizing IR field, as applied in the present section, is not as critical as accounting for time-dependent excited-state ionization in Sec. II. In the former case, there is only a slight improvement of the

agreement with the TDSE calculations. Meanwhile, according to the *ab initio* calculations, the intensity of the IR field required for the pulse formation due to ionization switching of the resonant interaction is one order of magnitude higher than that estimated from the tunneling formula [27]. This follows from the fact that the tunneling models overestimate the ionization rate in the barrier-suppression regime [57,58]. As seen in Fig. 6(b), which plots the Fourier transform of the output XUV radiation, for the chosen parameters of the IR field, the generalized analytical solution (18) provides good agreement with the numerical results both in time- and frequency-domain representations.

Let us further examine the possibilities to reduce the pulse duration via reducing the wavelength of the IR field (leading to shrinking of the overall time scale) or via increasing the intensity of the IR field (leading to the speedup of the excited-state ionization). Figures 7 and 8 represent the case of the helium atoms irradiated by the IR field with the same intensity as in Fig. 6, $I_{IR} = 1.5 \times 10^{14}$ W/cm^2, but with shorter wavelengths. The atoms are simultaneously exposed to the

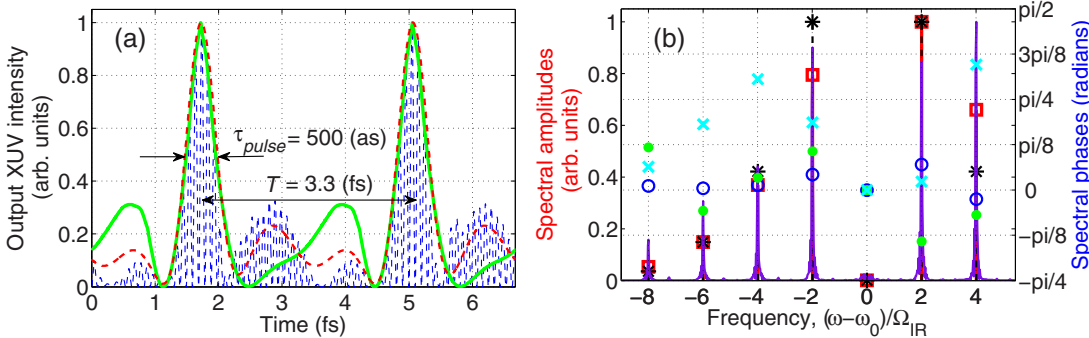FIG. 7. (a) Same as Fig. 6(a), but for IR field with wavelength $\lambda_{IR} = 2\,\mu$m. The dimensionless parameters in the analytical solutions are $P_\omega^{(2)} = 4.0$, $P_\gamma^{(2)} = 4.6$, $\bar{\gamma}_{min}/\Omega = 0.14$, $\bar{\gamma}_{max}/\Omega = 1.5$, and $\Omega\Delta t_{zero} = 0.25\pi$. (b) Fourier transform of the output XUV radiation corresponding to the time dependence in (a). Designations are the same as in Fig. 6(b).
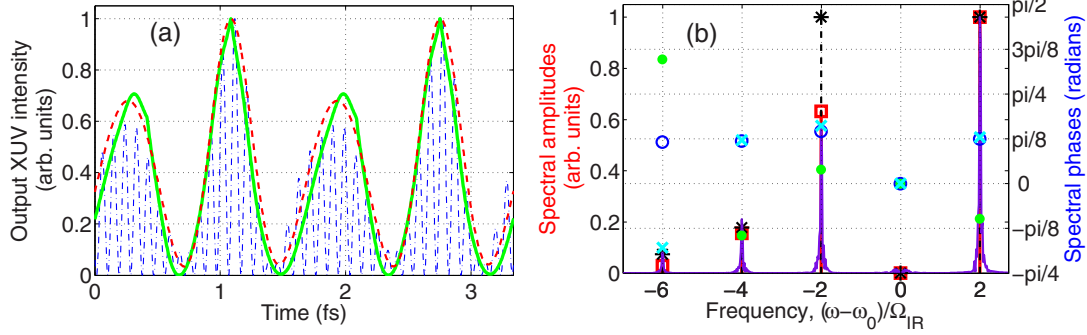
FIG. 8. (a) Same as Fig. 6(a), but for IR field with wavelength $\lambda_{IR} = 1 \, \mu m$. The dimensionless parameters in the analytical solutions are $P_\omega^{(2)} = 1.0$, $P_\gamma^{(2)} = 1.2$, $\bar{\gamma}_{\min}/\Omega = 0.22$, $\bar{\gamma}_{\max}/\Omega = 0.88$, and $\Omega \Delta t_{\text{zero}} = 0.4\pi$. (b) Fourier transform of the output XUV radiation corresponding to the time dependence in (a). Designations are the same as in Fig. 6(b).

resonant XUV radiation. Figure 7 corresponds to the IR field with wavelength $\lambda_{IR} = 2 \, \mu m$. In this case, the output XUV radiation has a form of a pulse train with pulse duration $\tau_{\text{pulse}} = 500$ as and repetition period $T = 3.3$ fs. As seen from the comparison of Figs. 7 and 6, the twofold reduction of the wavelength of the IR field expectedly leads to a proportional reduction of the pulse repetition period. However, the duration of the pulses is only slightly reduced. This is due to the fact that the pulse duration is determined by the ionization-limited lifetime of the resonant excited state $|2\rangle$, which approximately equals Δt_{zero} and is nearly the same for 2- and 4-μm IR fields of the same intensity. In Fig. 8 we show the time dependence of the intensity and the spectrum of the output XUV radiation for the case of helium irradiated by the resonant XUV field and the IR field with wavelength $\lambda_{IR} = 1 \, \mu m$. The resonant component of the output XUV radiation is suppressed. For such a short wavelength of the IR field, the pulse formation does not occur, since the intensity of the IR field is not high enough to provide complete atomic ionization from the resonant excited state during the half cycle of the IR field (which is four times shorter compared to the half cycle of the 4-μm IR field assumed in Fig. 6). Correspondingly, ionization never switches off the resonant interaction between the XUV field and the atoms, and the necessary condition for pulse formation [37] is not met. As

follows from Figs. 7 and 8, for all the considered wavelengths of the IR field, the analytical solutions (17) and (18), and (20)–(23), are in rather good agreement with the results of TDSE calculations. This is due to the quasistatic nature of excited-state ionization in the barrier-suppression regime [57]. However, the generalized solution (17) and (18) better reproduces the results of *ab initio* calculations due to a proper description of time dependence of the excited-state ionization rate in the barrier-suppression regime and accounting for the sub-laser-cycle quadratic Stark effect.

Figures 9 and 10 show the results of the study aimed to examine the possibilities to reduce the pulse duration via increasing the intensity of the IR field. The wavelength of the IR field is fixed to $\lambda_{IR} = 4 \, \mu m$. Figure 9 corresponds to the laser intensity $I_{IR} = 4 \times 10^{14} \, \text{W/cm}^2$. As seen from the comparison of this figure with Fig. 6, the increase of the IR field intensity leads to a slight reduction of the pulse duration, from $\tau_{\text{pulse}} = 600$ as to $\tau_{\text{pulse}} = 550$ as, and suppression of the pulse pedestal. The reason for such a slow decrease of the pulse duration with increasing laser-field intensity is that the duration of pulses is predominantly determined by the length of the time interval near zero crossing of the IR field during which the ionization rate is negligible and the resonant interaction occurs rather than by the peak ionization rate.
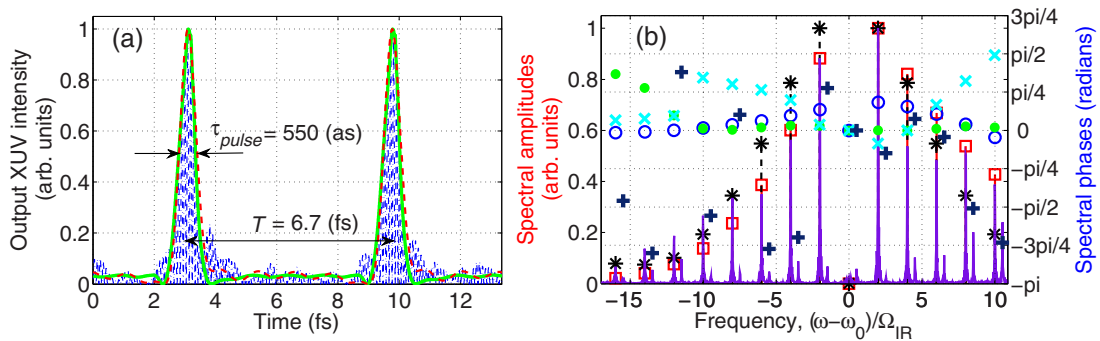

FIG. 9. (a) Same as Fig. 6(a), but for IR field with intensity $I_{IR} = 4 \times 10^{14} \, \text{W/cm}^2$. The dimensionless parameters in the analytical solutions are $P_\omega^{(2)} = 25$, $P_\gamma^{(2)} = 20.7$, $\bar{\gamma}_{\min}/\Omega = 0.24$, $\bar{\gamma}_{\max}/\Omega = 6.2$, and $\Omega \Delta t_{\text{zero}} = 0.16\pi$. (b) Fourier transform of the output XUV radiation corresponding to the time dependence in (a). Designations are the same as in Fig. 6(b). (i) Cyan crosses and (ii) dark blue pluses show the results of the TDSE solution for the phases of spectral components at (i) the combinational frequencies, $\omega = \omega_0 + n\Omega$, $n = 0, \pm 1, \pm 2, \ldots$, and (ii) the high-order harmonics of the IR field, $\omega = (2k + 1)\Omega$, $k = 1, 2, \ldots$, respectively.
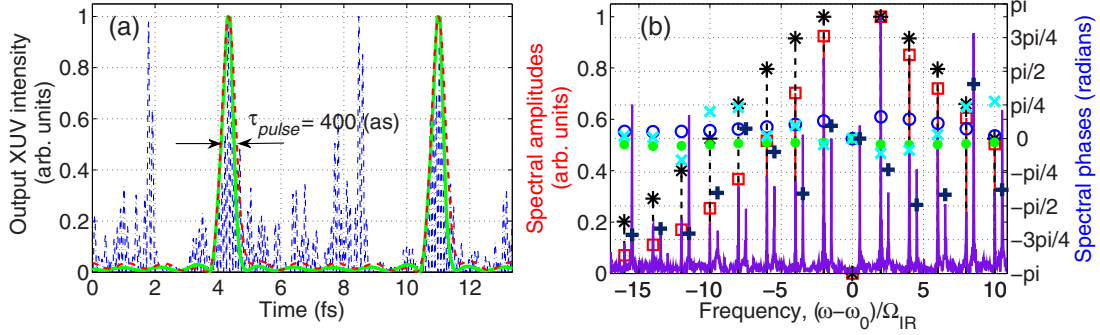
FIG. 10. (a) Same as Fig. 6(a), but for IR field with intensity $I_{IR} = 8 \times 10^{14}$ W/cm^2. The dimensionless parameters in the analytical solutions are $P_\omega^{(2)} = 50$, $P_\gamma^{(2)} = 51$, $\bar{\gamma}_{min} = 0.66\Omega$, $\bar{\gamma}_{max} = 11.2\Omega$, and $\Delta t_{zero} = 0.1\pi/\Omega$. (b) Fourier transform of the output XUV radiation corresponding to the time dependence in (a). Designations are the same as in Fig. 9(b).

With increasing intensity of the IR field, this time interval is shortened quite slowly; therefore, the dependence of the pulse duration on the laser intensity is weak. In Fig. 10 we show the time dependence of intensity and the spectrum of the output XUV radiation after suppression of its resonant component for the case of the IR field with wavelength $\lambda_{IR} = 4\,\mu$m and intensity $I_{IR} = 8 \times 10^{14}$ W/cm^2. As follows from Fig. 10(a), the duration of pulses produced from the resonant radiation is reduced to $\tau_{pulse} = 400$ as. However, along with the pulses of resonantly scattered radiation, the other spikes appear due to HHG of the modulating IR field. Indeed, for the parameters of the XUV and IR fields related to this case, there are two distinct groups of spectral components of comparable amplitudes; see Fig. 10(b). The first group corresponds to the combinational frequencies of the XUV and IR fields, $\omega = \omega_0 + 2n\Omega$, $n = \pm 1, \pm 2, \ldots$, while the second group is the high-order harmonics of the IR field, $\omega = (2k + 1)\Omega$, $k = \pm 1, \pm 2, \ldots$ Unless the depletion of the ground state is considerable, the HHG yield is proportional to the ground-state ionization rate and, thus, grows exponentially with increasing IR field strength. Even a small increase in laser intensity beyond the above-mentioned value will lead to domination of the high-harmonic signal over the resonantly scattered radiation. Thus, for the intensities of the incident XUV radiation discussed here, the ultimate intensity of the IR field suitable for few-cycle pulse formation from XUV radiation via ionization switching of its resonant interaction with atoms is limited to the value at which ionization from the ground atomic state, leading to HHG of the IR field, becomes significant. At the same time, as follows from the results of calculations based on few-level and quasistatic approximations, the ionization-switching mechanism works even if the intensity of the incident XUV radiation reaches a quarter intensity of the modulating IR field [40]. In such a case, HHG via atomic ionization from the ground state does not hamper sub-fs pulse formation from XUV radiation due to the ionization-switching mechanism. Instead, ultimate capabilities for the pulse formation are limited by depletion of the atomic ground state through (i) direct ionization by the IR field and (ii) resonant excitation by the XUV radiation followed by excited-state ionization by the IR field.

In summary, based on the *ab initio* solution of the TDSE, we have shown the possibility to produce trains of $\sim$500-as

pulses from the XUV radiation with wavelength 58.4 nm via ionization switching of its resonant interaction with the helium atoms dressed by the IR field with wavelength 2–4 μm and intensity $(1.5-4) \times 10^{14}$ W/cm^2. Experimentally, the IR field with these parameters can be generated by a parametric laser system [50], while the resonant XUV radiation can be produced, for example, via the resonantly enhanced HHG of Ti:sapphire laser field in an InP plasma plume [23,25]. As discussed in [37,38], few-cycle pulse formation via the ionization-switching mechanism can be implemented in arbitrary atomic gas. In particular, TDSE calculations show the possibility to produce pulses similar to those plotted in Figs. 6–10 from XUV radiation with wavelength 121.6 nm in atomic hydrogen dressed by the IR field with wavelength 4 μm and intensity of the order of 10^{14} W/cm^2. The pulses of shorter duration can be produced using ions with higher ionization potential from the ground state. It is worth noting that few-cycle pulses similar to those discussed above can be produced via the ionization-switching mechanism in media with lower ionization potential also. In such a case, the carrier frequency of the pulses can be considerably lower, which would make them especially valuable for nonionizing steering and probing transient physical, chemical, and biological intra-atomic and intramolecular processes in various media.

IV. CONCLUSION

In the present paper, we have studied ultimate capabilities for few-cycle pulse formation from XUV radiation via the resonant interaction with IR-field-dressed atoms. This study was carried out on the basis of a full time-dependent Schrödinger equation. Taking into account all the multiphoton processes in the considered systems in the single-active-electron approximation, we have confirmed the possibilities for few-femtosecond pulse formation via the linear Stark effect in atomic hydrogen, as well as attosecond pulse formation via quasistatic excited-state ionization in helium. We have found the ultimate limitations on the parameters (the minimum wavelength and the maximum intensity) of the IR field suitable for the few-cycle pulse formation, as well as characteristics of the produced pulses. Particularly, in the case of XUV pulse formation via the linear Stark effect in atomic hydrogen, the output pulses can be as short as 1 fs, which is two times

shorter than predicted by the previous calculations based on the three-level approximation [36]; the laser intensity can be up to 10^{13} W/cm^2, while the laser wavelength can be as short as $4\,\mu$m. The ionization switching of the resonant interaction in helium requires the laser intensity up to 4×10^{14} W/cm^2, whereas the laser wavelength can be as short as $2\,\mu$m; the duration of output pulses is $\sim$500 as.

In order to analyze the results of *ab initio* calculations, we derived the generalized analytical solution, which takes into account the interplay between sub-IR-field-cycle variations of position and width of the resonant atomic energy levels due to the Stark effect and excited-state ionization, respectively. The derived analytical solution is in good agreement with the results of TDSE calculations both in the case of atomic hydrogen in a relatively weak IR field and in the case of helium in a strong IR field. Thus such a solution can be used for the analysis of the various resonant phenomena in a system of IR-field-dressed atoms. Based on a comparison of the numerical and analytical solutions, we revealed the limitations of the considered method for few-cycle pulse formation. In particular, the possibility of shortening the pulses produced via the linear Stark effect in atomic hydrogen by increasing the intensity of the IR field is limited by the growing role of exited-state ionization, which leads to a misalignment of phases of the generated sidebands. The ultimate intensity of the IR field suitable for attosecond pulse formation via rapid quasistatic ionization from the resonant excited state of helium is limited to a value at which atomic ionization from the ground state becomes significant, entailing HHG and blurring the produced pulses by the high-harmonic signal. To overcome both these limitations and produce shorter pulses, we proposed the use of the medium of hydrogenlike or heliumlike ions with higher ionization potentials from both the ground and the excited states. We also pointed out the possibility to produce few-cycle pulses with lower carrier frequency, in a close proximity to resonances of various atomic and molecular systems, using media with lower ionization potential. The paper contains accurate estimation of wavelengths and intensities of XUV and IR fields suitable for experimental implementation of the method. The proposed method provides a unique tool for nonionizing steering of electronic processes inside atoms, molecules, and solids at the few-femtosecond and attosecond time scales, thus extending the capabilities of attosecond science. Furthermore, the method is very promising for transformation of the picosecond pulses produced by the x-ray plasma lasers into subfemtosecond pulses, which could widely extend the applications of such lasers for element selective imaging of the fast dynamical processes in biochemistry and material sciences.

[1] P. M. Paul, E. S. Toma, P. Breger, G. Mullot, F. Auge, Ph. Balcou, H. G. Muller, and P. Agostini, Observation of a train of attosecond pulses from high harmonic generation, Science **292**, 1689 (2001).

[2] M. Hentschel, R. Kienberger, Ch. Spielmann, G. A. Reider, N. Milosevic, T. Brabec, P. Corkum, U. Heinzmann, M. Drescher, and F. Krausz, Attosecond metrology, Nature **414**, 509 (2001).

[3] F. Krausz and M. Ivanov, Attosecond physics, Rev. Mod. Phys. **81**, 163 (2009).

[4] L. Gallmann, C. Cirelli, and U. Keller, Attosecond science: Recent highlights and future trends, Annu. Rev. Phys. Chem. **63**, 447 (2012).

[5] P. Salières, A. Maquet, S. Haessler, J. Caillat, and R. Taïeb, Imaging orbitals with attosecond and Ångström resolutions: Toward attochemistry? Rep. Prog. Phys. **75**, 062401 (2012).

[6] L. Gallmann, J. Herrmann, R. Locher, M. Sabbar, A. Ludwig, M. Lucchini, and U. Keller, Resolving intra-atomic electron dynamics with attosecond transient absorption spectroscopy, Mol. Phys. **111**, 2243 (2013).

[7] S. R. Leone, C. W. McCurdy, J. Burgdörfer, L. S. Cederbaum, Z. Chang, N. Dudovich, J. Feist, C. H. Greene, M. Ivanov, R. Kienberger, U. Keller, M. F. Kling, Z.-H. Loh, T. Pfeifer, A. N. Pfeiffer, R. Santra, K. Schafer, A. Stolow, U. Thumm, and M. J. J. Vrakking, What will it take to observe processes in 'real time'? Nat. Photon. **8**, 162 (2014).

[8] M. Chini, K. Zhao, and Z. Chang, The generation, characterization and applications of broadband isolated attosecond pulses, Nat. Photon. **8**, 178 (2014).

[9] F. Krausz and M. I. Stockman, Attosecond metrology: From electron capture to future signal processing, Nat. Photon. **8**, 205 (2014).

[10] A. H. Zewail, Femtochemistry: Atomic-scale dynamics of the chemical bond, J. Phys. Chem. A **104**, 5660 (2000).

[11] P. Johnsson, J. Mauritsson, T. Remetter, A. L'Huillier, and K. J. Schafer, Attosecond Control of Ionization by Wave-Packet Interference, Phys. Rev. Lett. **99**, 233001 (2007).

[12] M. Swoboda, T. Fordell, K. Klünder, J. M. Dahlström, M. Miranda, C. Buth, K. J. Schafer, J. Mauritsson, A. L'Huillier, and M. Gisselbrecht, Phase Measurement of Resonant Two-Photon Ionization in Helium, Phys. Rev. Lett. **104**, 103003 (2010).

[13] X. M. Tong, P. Ranitovic, C. L. Cocke, and N. Toshima, Mechanisms of infrared-laser-assisted atomic ionization by attosecond pulses, Phys. Rev. A **81**, 021404(R) (2010).

[14] S. Gilbertson, M. Chini, X. Feng, S. Khan, Y. Wu, and Z. Chang, Monitoring and Controlling the Electron Dynamics in Helium with Isolated Attosecond Pulses, Phys. Rev. Lett. **105**, 263003 (2010).

[15] N. Shivaram, H. Timmers, X.-M. Tong, and A. Sandhu, Attosecond-Resolved Evolution of a Laser-Dressed Helium Atom: Interfering Excitation Paths and Quantum Phases, Phys. Rev. Lett. **108**, 193002 (2012).

[16] C. Ott, A. Kaldun, P. Raith, K. Meyer, M. Laux, J. Evers, C. H. Keitel, C. H. Greene, and T. Pfeifer, Lorentz meets Fano in spectral line shapes: A universal phase and its laser control, Science **340**, 716 (2013).

[17] M. Chini, B. Zhao, H. Wang, Y. Cheng, S. X. Hu, and Z. Chang, Subcycle ac Stark Shift of Helium Excited States Probed with Isolated Attosecond Pulses, Phys. Rev. Lett. **109**, 073601 (2012).

[18] M. Chini, X. Wang, Y. Cheng, Y. Wu, D. Zhao, D. A. Telnov, S.-I. Chu, and Z. Chang, Sub-cycle oscillations in virtual states brought to light, Sci. Rep. **3**, 1105 (2013).

[19] P. Ranitovic, X. M. Tong, C. W. Hogle, X. Zhou, Y. Liu, N. Toshima, M. M. Murnane, and H. C. Kapteyn, Controlling the XUV Transparency of Helium Using Two-Pathway Quantum Interference, Phys. Rev. Lett. **106**, 193008 (2011).

[20] T. R. Akhmedzhanov, A. Antonov, and Olga Kocharovskaya, Coherent forward scattering of γ-ray and XUV radiation in the medium with the modulated quasi-resonant transition, J. Phys. B: At., Mol. Opt. Phys. **49**, 205602 (2016).

[21] E. J. Takahashi, P. Lan, O. D. Mücke, Y. Nabekawa, and K. Midorikawa, Attosecond nonlinear optics using gigawatt-scale isolated attosecond pulses, Nat. Commun. **4**, 2691 (2013).

[22] M. Chini, X. Wang, Y. Cheng, H. Wang, Y. Wu, E. Cunningham, P.-C. Li, J. Heslar, D. A. Telnov, S.-I Chu, and Z. Chang, Coherent phase-matched VUV generation by field-controlled bound states, Nat. Photon. **8**, 437 (2014).

[23] D. C. Yost, T. R. Schibli, J. Ye, J. L. Tate, J. Hostetter, M. B. Gaarde, and K. J. Schafer, Vacuum-ultraviolet frequency combs from below-threshold harmonics, Nat. Phys. **5**, 815 (2009).

[24] R. A. Ganeev, H. Singhal, P. A. Naik, V. Arora, U. Chakravarty, J. A. Chakera, R. A. Khan, I. A. Kulagin, P. V. Redkin, M. Raghuramaiah, and P. D. Gupta, Harmonic generation from indium-rich plasmas, Phys. Rev. A **74**, 063824 (2006).

[25] R. A. Ganeev, L. B. Elouga Bom, T. Ozaki, and P. V. Redkin, Maximizing the yield and cutoff of high-order harmonic generation from plasma plume, J. Opt. Soc. Am. B **24**, 2770 (2007).

[26] R. A. Ganeev, *High-Order Harmonic Generation in Laser Plasma Plumes* (Imperial College Press, London, 2012).

[27] J. J. Rocca, Table-top soft x-ray lasers, Rev. Sci. Instrum. **70**, 3799 (1999).

[28] H. Daido, Review of soft x-ray laser researches and developments, Rep. Prog. Phys. **65**, 1513 (2002).

[29] S. Suckewer and P. Jaeglé, X-ray laser: past, present, and future, Laser Phys. Lett. **6**, 411 (2009).

[30] M. Nishikino and T. Kawachi, Soft-x-ray sources: x-ray laser plasma amplifiers, Nat. Photon. **8**, 352 (2014).

[31] Y. V. Radeonychev, A. Polovinkin, and O. Kocharovskaya, Extremely Short Pulses via Stark Modulation of the Atomic Transition Frequencies, Phys. Rev. Lett. **105**, 183902 (2010).

[32] V. A. Polovinkin, Y. V. Radeonychev, and O. Kocharovskaya, Few-cycle attosecond pulses via periodic resonance interaction with hydrogenlike atoms, Opt. Lett. **36**, 2296 (2011).

[33] N. B. Delone and V. P. Krainov, AC Stark shift of atomic energy levels, Phys. Usp. **42**, 669 (1999).

[34] V. S. Popov, Tunnel and multiphoton ionization of atoms and ions in a strong laser field (Keldysh theory), Phys. Usp. **47**, 855 (2004).

[35] S. V. Popruzhenko, Keldysh theory of strong field ionization: History, applications, difficulties and perspectives, J. Phys. B: At., Mol. Opt. Phys. **47**, 204001 (2014).

[36] V. A. Antonov, Y. V. Radeonychev, and O. Kocharovskaya, Formation of ultrashort pulses via quantum interference between Stark-split atomic transitions in a hydrogenlike medium, Phys. Rev. A **88**, 053849 (2013).

[37] V. A. Antonov, T. R. Akhmedzhanov, Y. V. Radeonychev, and O. Kocharovskaya, Attosecond pulse formation via switching of resonant interaction by tunnel ionization, Phys. Rev. A **91**, 023830 (2015).

[38] V.A. Antonov, Y.V. Radeonychev, and O. Kocharovskaya, Formation of a Single Attosecond Pulse via Interaction of Resonant Radiation with a Strongly Perturbed Atomic Transition, Phys. Rev. Lett. **110**, 213903 (2013).

[39] Y. Mairesse, A. de Bohan, L. J. Frasinski, H. Merdji, L. C. Dinu, P. Monchicourt, P. Breger, M. Kovačev, R. Taïeb, B. Carré, H. G. Muller, P. Agostini, and P. Salières, Attosecond synchronization of high-harmonic soft x-rays, Science **302**, 1540 (2003).

[40] Y. V. Radeonychev, A. Antonov, and O. A. Kocharovskaya, Resonant formation of few-cycle pulses by hydrogen-like atoms with time-dependent resonance, Laser Phys. **23**, 085303 (2013).

[41] P. Tzallas, E. Skantzakis, L. A. A. Nikolopoulos, G. D. Tsakiris, and D. Charalambidis, Extreme-ultraviolet pump-probe studies of one-femtosecond-scale electron dynamics, Nat. Phys. **7**, 781 (2011).

[42] D. V. Korobkin, C. H. Nam, S. Suckewer, and A. Goltsov, Demonstration of Soft X-Ray Lasing to Ground State in Li III, Phys. Rev. Lett. **77**, 5206 (1996).

[43] B. A. Reagan, M. Berrill, K. A. Wernsing, C. Baumgarten, M. Woolston, and J. J. Rocca, High-average-power, 100-Hz-repetition-rate, tabletop soft-x-ray lasers at sub-15-nm wavelengths, Phys. Rev. A **89**, 053820 (2014).

[44] P. W. Wachulak, A. Bartnik, H. Fiedorowicz, P. Rudawski, R. Jarocki, J. Kostecki, and M. Szczurek, "Water window" compact, table-top laser plasma soft X-ray sources based on a gas puff target, Nucl. Instrum. Methods Phys. Res., Sect. B **268**, 1692 (2010).

[45] K. Hoffmann, B. Murphy, B. Erk, A. Helal, N. Kandadai, J. Keto, and T. Ditmire, High intensity femtosecond XUV pulse interactions with atomic clusters, High Energy Density Phys. **6**, 185 (2010).

[46] L. Yue and L. B. Madsen, Characterization of Molecular Breakup by Very Intense Femtosecond XUV Laser Pulses, Phys. Rev. Lett. **115**, 033001 (2015).

[47] E. V. Vanin, A. V. Kim, A. M. Sergeev, and M. C. Downer, Excitation of ultrashort bursts of harmonics of the radiation during ionization of a gas by an intense light pulse, Pis'ma Zh. Eksp. Teor. Fiz. **58**, 964 (1993) [JETP Lett. **58**, 900 (1993)].

[48] T. Brabec and F. Krausz, Nonlinear Optical Pulse Propagation in the Single-Cycle Regime, Phys. Rev. Lett. **78**, 3282 (1997).

[49] X.-M. Tong and S.-I Chu, Theoretical study of multiple high-order harmonic generation by intense ultrashort pulsed laser fields: A new generalized pseudospectral time-dependent method, Chem. Phys. **217**, 119 (1997).

[50] G. Andriukaitis, T. Balčiūnas, S.Ališauskas, A. Pugžlys, A. Baltuška, T. Popmintchev, M.-C. Chen, M. M. Murnane, and H. C. Kapteyn, 90 GW peak power few-cycle mid-infrared pulses from an optical parametric amplifier, Opt. Lett. **36**, 2755 (2011).

[51] O. J. Luiten, H. G. C. Werij, M. W. Reynolds, I. D. Setija, T. W. Hijmans, and J. T. M. Walraven, VUV spectroscopy of magnetically trapped atomic hydrogen, Appl. Phys. B **59**, 311 (1994).

[52] C. E. M. Strauss and D. J. Funk, Broadly tunable difference-frequency generation of VUV using two-photon resonances in H_2 and Kr, Opt. Lett. **16**, 1192 (1991).

[53] P.-C. Li, C. Laughlin, and S.-I Chu, Generation of isolated sub-20-attosecond pulses from He atoms by two-color midinfrared laser fields, Phys. Rev. A **89**, 023431 (2014).

[54] L. Benassi and V. Grecchi, Resonances in the Stark effect and strongly asymptotic approximants, J. Phys. B: At. Mol. Phys. **13**, 911 (1980).

[55] V. V. Kolosov, Stark effect near the peak of the potential barrier, J. Phys. B: At. Mol. Phys. **16**, 25 (1983).

[56] G. L. Yudin and M. Yu. Ivanov, Nonadiabatic tunnel ionization: Looking inside a laser cycle, Phys. Rev. A **64**, 013409 (2001).

[57] D. Bauer and P. Mulser, Exact field ionization rates in the barrier-suppression regime from numerical time-dependent Schrödinger-equation calculations, Phys. Rev. A **59**, 569 (1999).

[58] X. M. Tong and C. D. Lin, Empirical formula for static field ionization rates of atoms and molecules by lasers in the barrier-suppression regime, J. Phys. B: At., Mol. Opt. Phys. **38**, 2593 (2005).

[59] http://hprc.tamu.edu/.